*Supporting Information*

# Constructing $FePSe_3$-$FeSe_2$ heterojunctions uniformly in Ketjen Black carbon matrix for superior potassium ion batteries

*Bi-Cui Chen[1], Xian Lu[1], Hou-Yang Zhong[1], Pei-Wen Huang[1], Ya-Nan Wu[1], Si-Yu Xu[1], Ke-Zhao Du[*,1] and Xiao-Hui Wu[*,1,2]*

1 College of Chemistry and Materials Science, Fujian Key Laboratory of Polymer Materials, Fujian Provincial Key Laboratory of Advanced Materials Oriented Chemical Engineering, Fujian Normal University, Fuzhou 350007, China.

2 State Key Laboratory of Structural Chemistry, Fujian Institute of Research on the Structure of Matter, Chinese Academy of Sciences, Fuzhou, Fujian 350002, China.

**Table S1.** The results of ICP-OES of $FePSe_3$-$FeSe_2$/C composite.

| **Elements** | **Mass percentage (%)** | **Molar percentage (%)** | **Molar ratio of $FePSe_3$ and $FeSe_2$** |
|---|---|---|---|
| Fe | 9.82 | 0.175 | 7.5: 1.0 |
| P | 4.77 | 0.154 | |
| Se | 39.42 | 0.499 | |

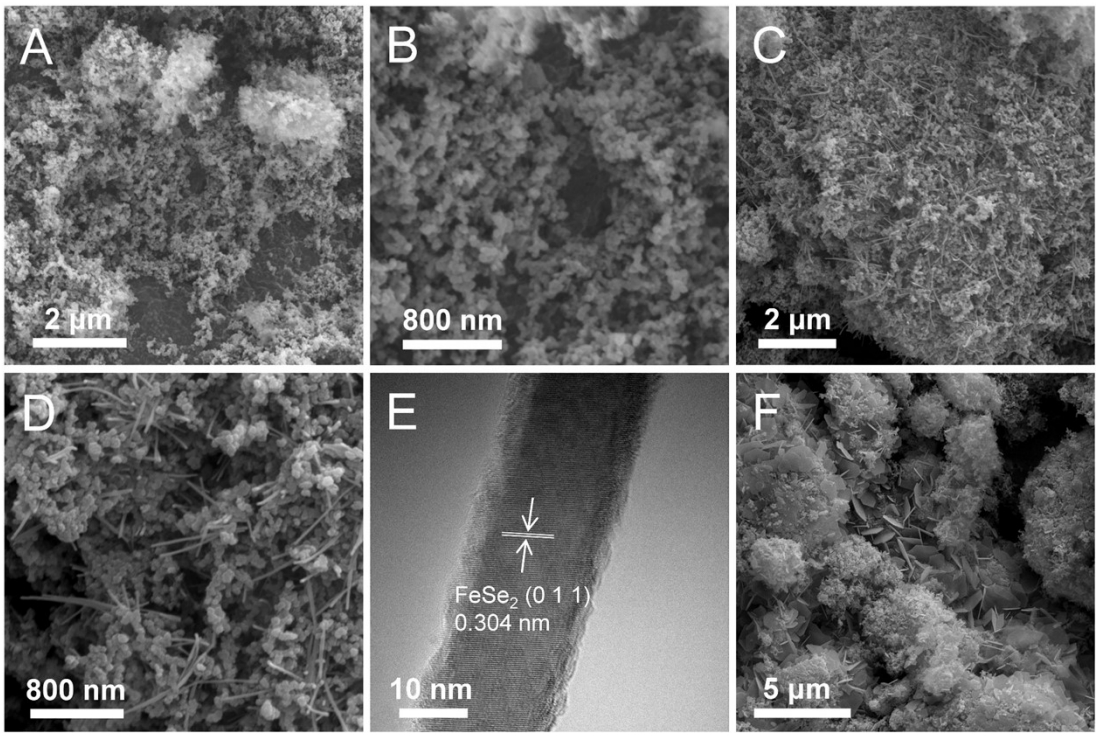


**Figure S1.** (A-B) SEM images of KB carbon. (C-D) SEM images and (E) HRTEM image of $FeSe_2$/C. (F) SEM image of $FePSe_3$/C.

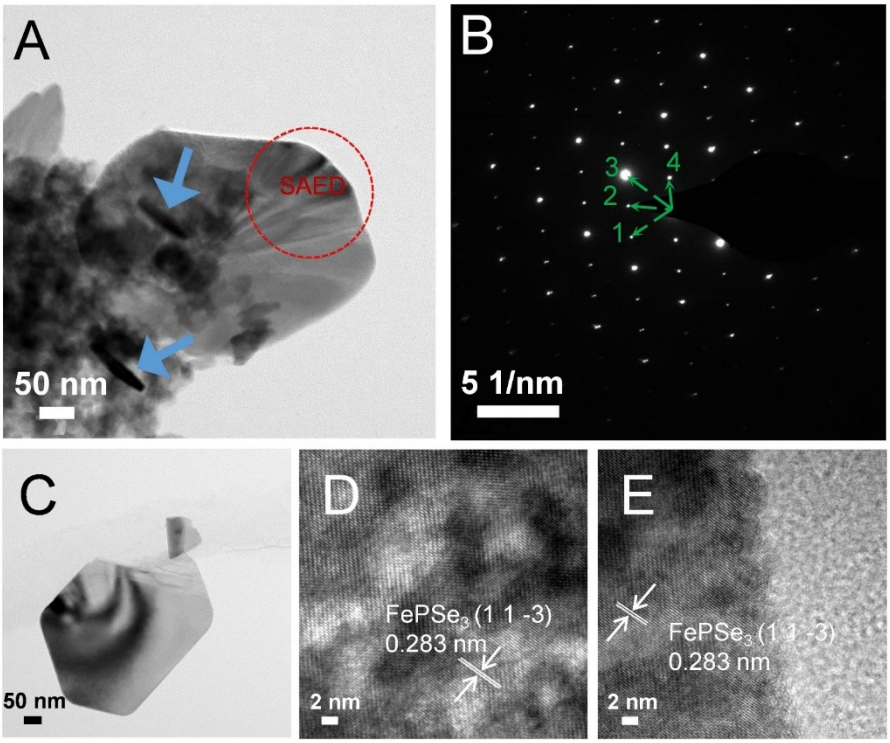


**Figure S2.** (A) TEM image, (B) SAED pattern, (C) TEM image and (D) & (E) HRTEM images of $FePSe_3$/C. In more details, points 1-4 marked in green in the SAED pattern correspond to the (-1 -1 -6), (0 -1 -5), (1 -1 -4) and (0 0 0) planes of $FePSe_3$, respectively.

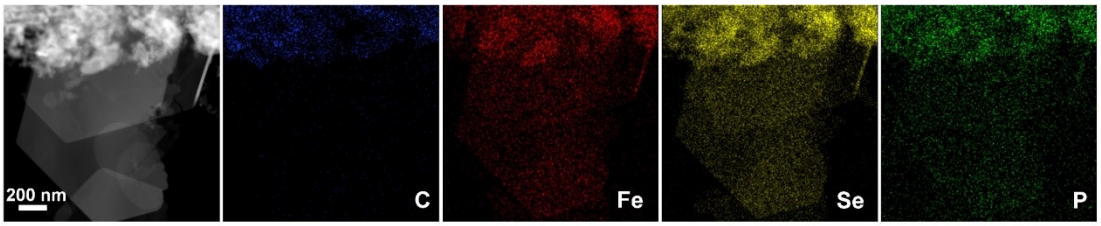


**Figure S3.** HAADF-STEM image with the corresponding EDS images of $FePSe_3$/C.

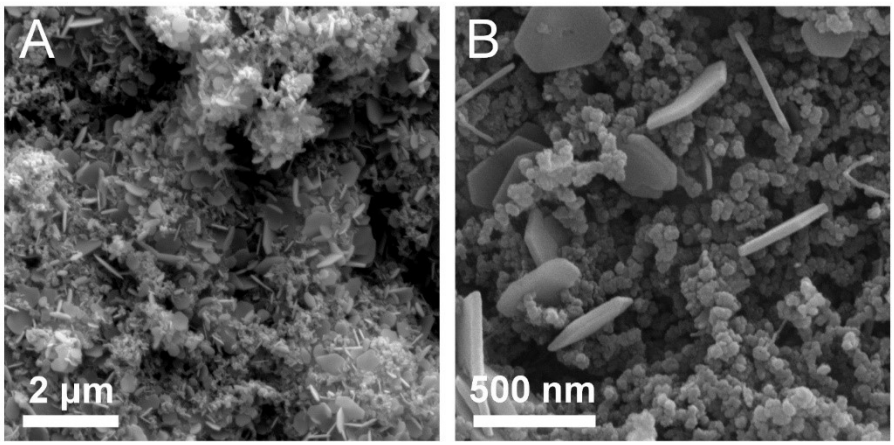


**Figure S4.** The high-resolution SEM images of $FePSe_3$-$FeSe_2$/C.

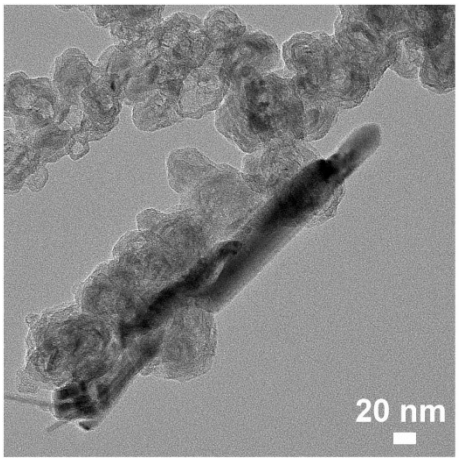


**Figure S5.** The TEM image of the side-view of $FePSe_3$-$FeSe_2$/C.

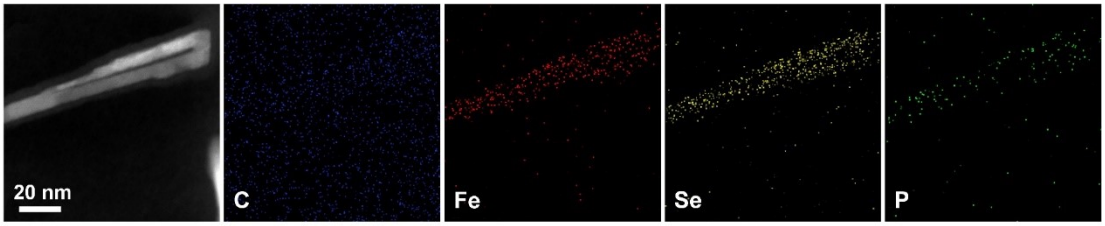


**Figure S6.** HAADF-STEM image with the corresponding EDS images of the side-view of $FePSe_3$-$FeSe_2$/C.

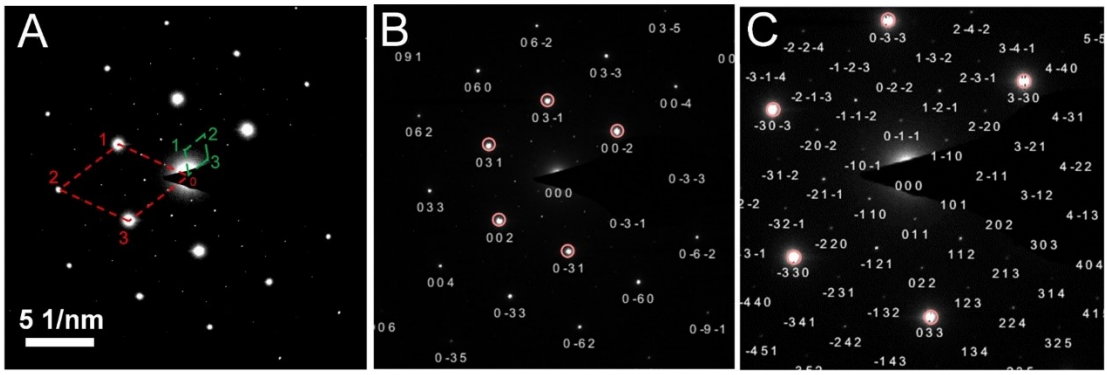


**Figure S7.** (A) SAED pattern of $FePSe_3$-$FeSe_2$/C. (B) The $FeSe_2$ crystal planes and (C) the $FePSe_3$ crystal planes corresponding to the diffraction spots in SAED.

This SAED pattern can be readily indexed as the 2D in-plane reflections of $FePSe_3$ with (-1 -1 1) zone axis direction and $FeSe_2$ with (1 0 0) zone axis direction. In more details, points 1-3 marked in green correspond to the (0 -1 -1), (1 -2 -1), and (1 -1 0) planes of $FePSe_3$, respectively, and the lattice planes of $FeSe_2$ represented by the red marked dots 1-3 in turn are (0 3 1), (0 3 3), and (0 0 2), respectively.

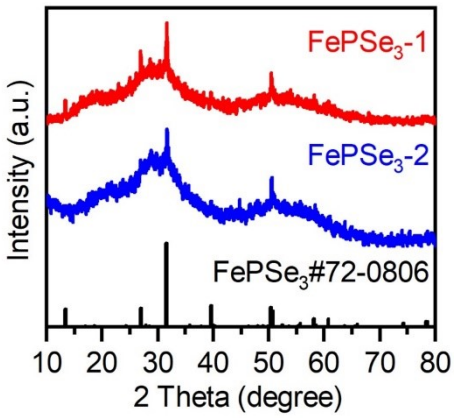


**Figure S8.** PXRD patterns of $FePSe_3$-1 and $FePSe_3$-2.

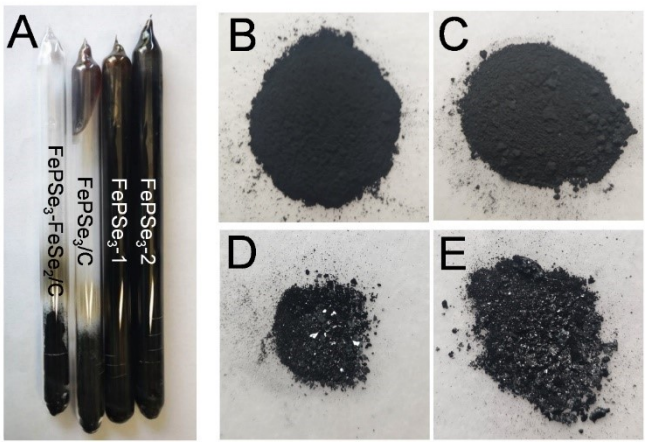


**Figure S9.** (A) The quartz tubes contain $FePSe_3$-$FeSe_2$/C, $FePSe_3$/C, $FePSe_3$-1 and $FePSe_3$-2 products in the order from left to right. (B) $FePSe_3$-$FeSe_2$/C products. (C) $FePSe_3$/C products. (D) $FePSe_3$-1 products. (E) $FePSe_3$-2 products.

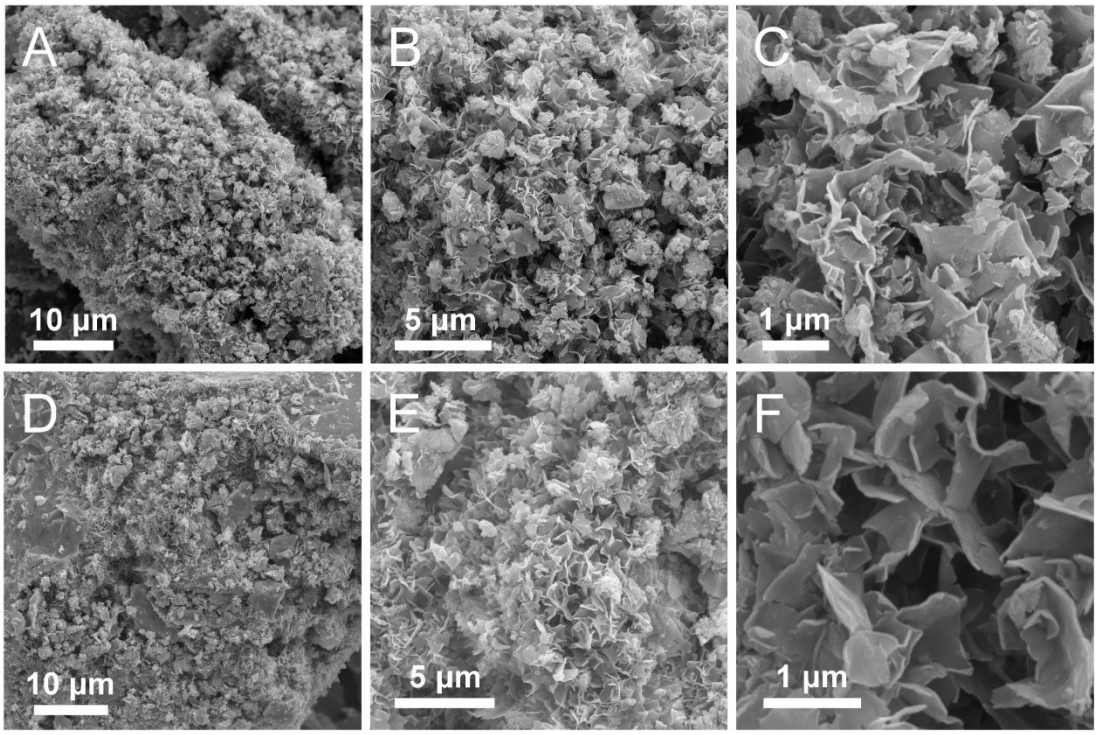


**Figure S10.** SEM images of (A-C) $FePSe_3$-1 and (D-F) $FePSe_3$-2.

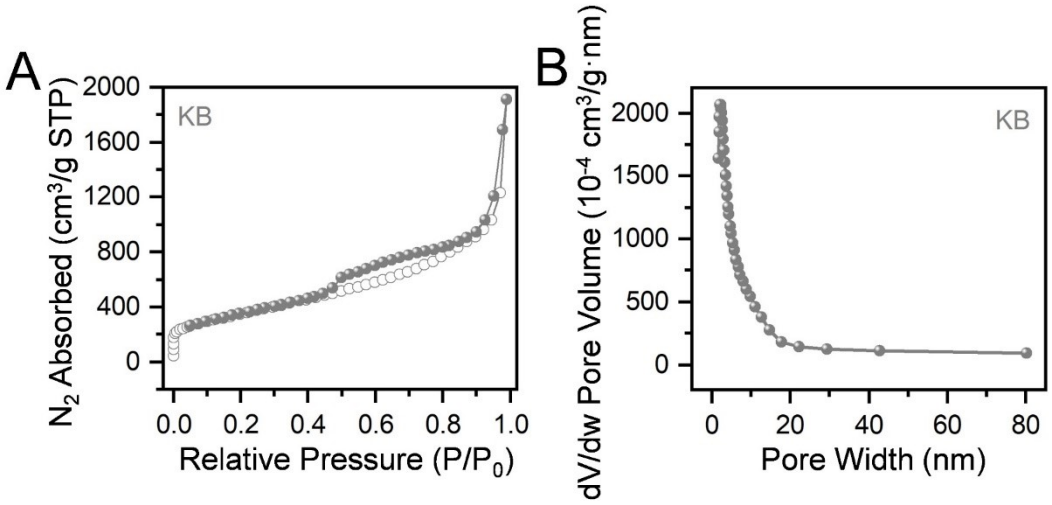


**Figure S11.** (A) $N_2$ adsorption-desorption isotherms and (B) the corresponding pore size distribution of KB carbon.

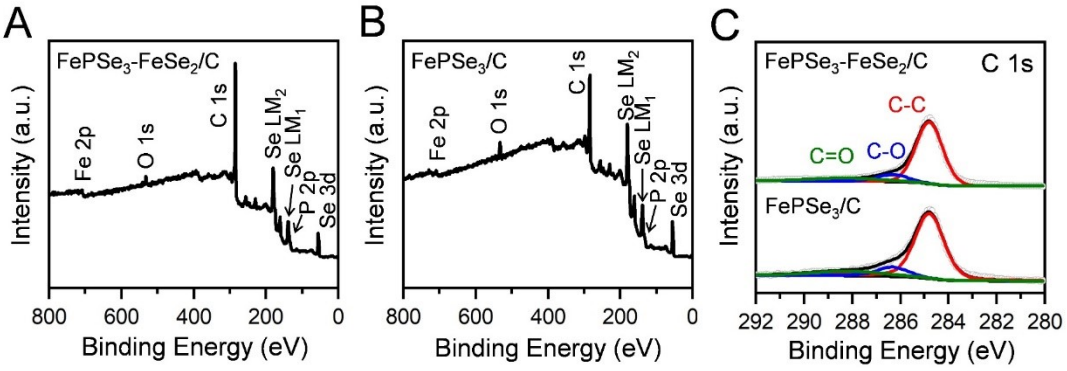


**Figure S12.** XPS survey spectra of (A) $FePSe_3$-$FeSe_2$/C and (B) $FePSe_3$/C. (C) High-resolution XPS C 1s spectra of $FePSe_3$-$FeSe_2$/C and $FePSe_3$/C.

**Table S2.** Brunauer Emmett Teller (BET) specific surface areas of KB, $FePSe_3$-$FeSe_2$/C and $FePSe_3$/C.

| **Sample** | **KB** | **$FePSe_3$-$FeSe_2$/C** | **$FePSe_3$/C** |
|---|---|---|---|
| **BET Surface Area ($m^2$/g)** | 1263.9 | 107.8 | 18.9 |

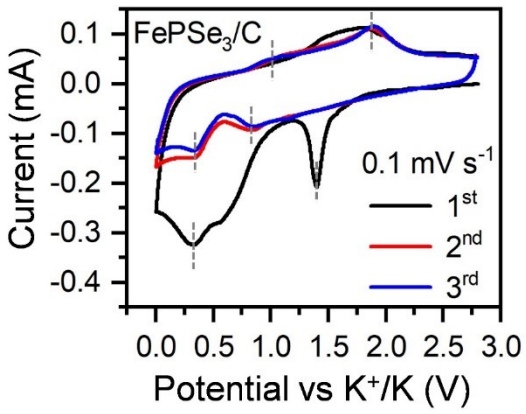


**Figure S13.** CV curves for initial three cycles of $FePSe_3$/C electrode for PIBs at 0.1 mV $s^{-1}$ between 0.005 and 2.8 V.

**Table S3.** The electrochemical reactions of $FePSe_3$-$FeSe_2$/C and $FeSe_2$/C with $K^+$ on anode.

| Sample | Potential | Reaction |
|---|---|---|
| **$FePSe_3$-$FeSe_2$/C** | Discharged to 1.40 V | $FePSe_3 + 6K^+ + 6e^- \rightarrow Fe + P + 3K_2Se$ |
| | Discharged to 1.20 V | $FeSe_2 + 4K^+ + 4e^- \rightarrow Fe + 2K_2Se$ |
| | Discharged to 0.48V | $3P + 4K^+ + 4e^- \rightarrow K_4P_3$ |
| | Charged to 1.04 V | $2Fe + 2K_2Se \rightarrow FeSe_2 + 4K^+ + 4e^-$ |
| | Charged to 1.74 V | $K_4P_3 + 9K_2Se + 3Fe \rightarrow 3FePSe_3 + 22K^+ + 22e^-$ |
| **$FePSe_3$/C** | Discharged to 1.40 V | $FePSe_3 + 6K^+ + 6e^- \rightarrow Fe + P + 3K_2Se$ |
| | Discharged to 0.32 V | $3P + 4K^+ + 4e^- \rightarrow K_4P_3$ |
| | Charged to 1.08 V | $K_4P_3 \rightarrow 3P + 4K^+ + 4e^-$ |
| | Charged to 1.80 V | $Fe + P + 3K_2Se \rightarrow FePSe_3 + 6K^+ + 6e^-$ |

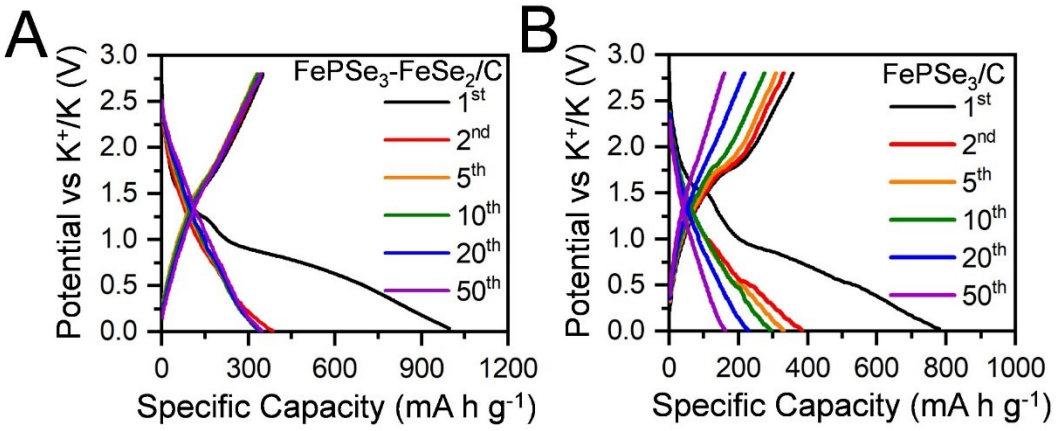


**Figure S14.** Charge−discharge profiles of (A) $FePSe_3$-$FeSe_2$/C and (B) $FePSe_3$/C at the current density of 0.1 A $g^{-1}$.

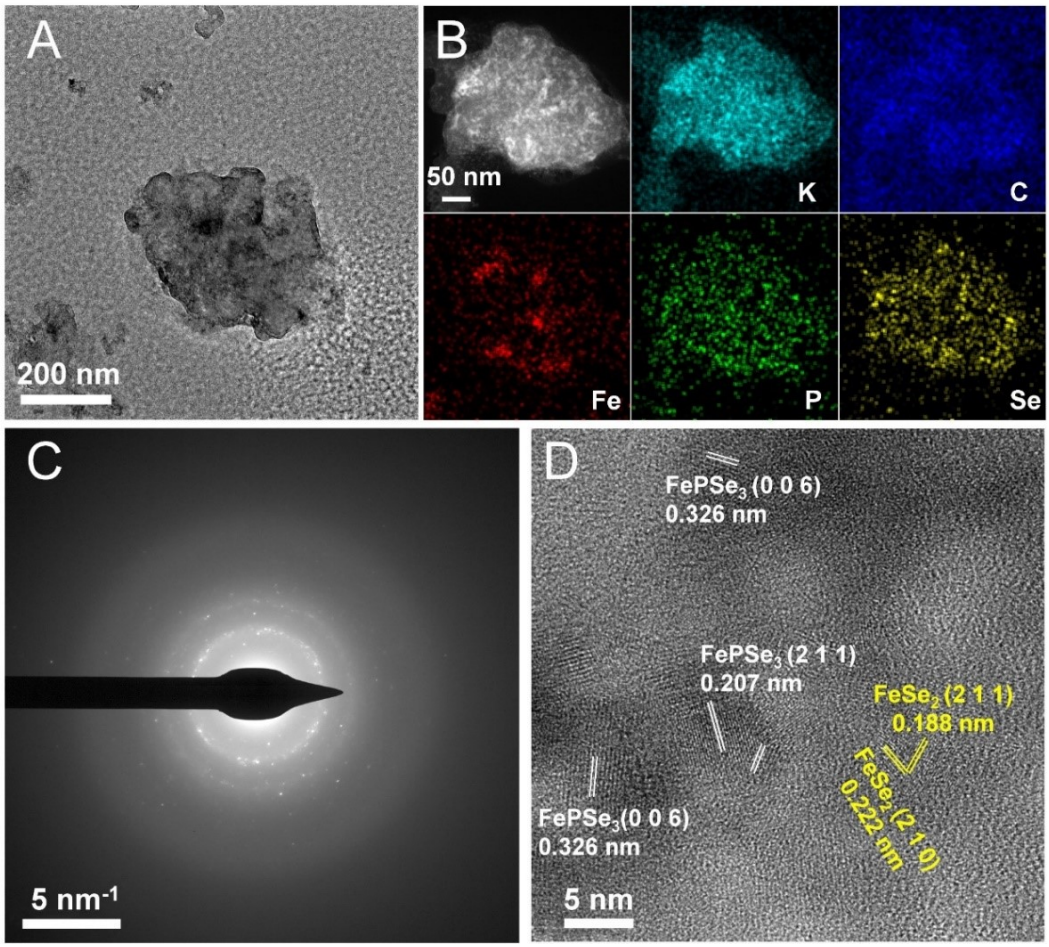

**Figure S15.** (A) TEM image, (B) HAADF-STEM image with the corresponding EDS images, (C) the SAED pattern and (D) HRTEM image of $FePSe_3$-$FeSe_2$/C at the current density of 0.1 A $g^{-1}$ after 260 cycles.

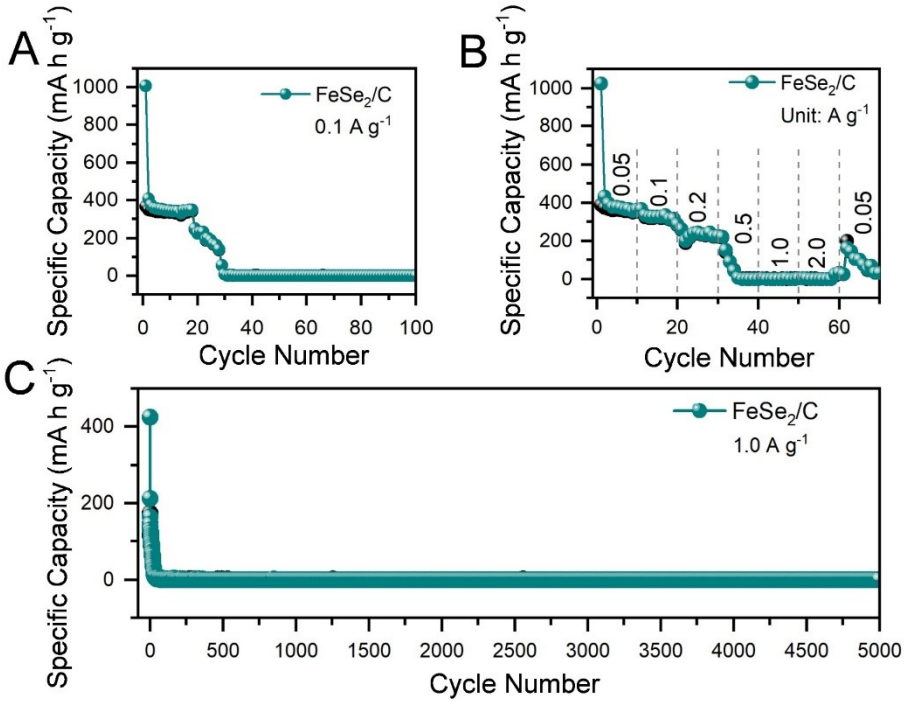


**Figure S16.** (A) Cycling performance, (B) rate performance and (C) long-term cyclic performance of $FeSe_2$/C electrodes in the voltage range of 0.005-2.8 V.

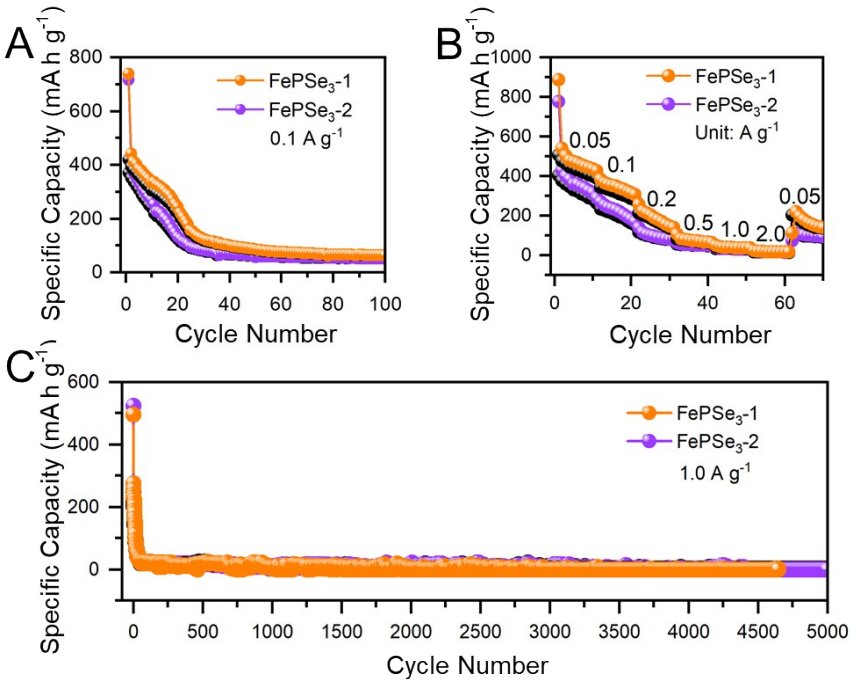


**Figure S17.** (A) Cycling performance of $FePSe_3$-1 and $FePSe_3$-2 electrodes at the current density of 0.1 A $g^{-1}$ in the range of 0.005-2.8 V. (B) Rate performance of $FePSe_3$-1 and $FePSe_3$-2 electrodes at various current densities from 0.05 to 2.0 A $g^{-1}$. (C) Long-term cyclic performance of $FePSe_3$-1 and $FePSe_3$-2 electrodes at 1.0 A $g^{-1}$.

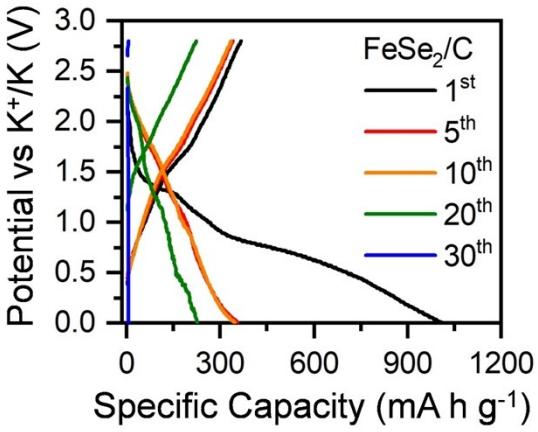


**Figure S18.** The galvanostatic charge/discharge profiles of $FeSe_2$/C at the current density of 0.1 A $g^{-1}$.

**Table S4.** Comparison of the cycling performance of $FePSe_3$-$FeSe_2$/C and other $FeSe_2$-based or $FePSe_3$-based materials for PIBs anodes.

| Material | Current density ($A\ g^{-1}$) | Cycle number | Capacity ($mA\ h\ g^{-1}$) | Mass loading ($mg\ cm^{-2}$) | Calculate based on | Ref |
|---|---|---|---|---|---|---|
| $FePSe_3$-$FeSe_2$/C | 0.1 | 100 | 352 | 1.0 | composite | This work |
| | 1.0 | 3700 | 224 | 0.7 | | |
| $FeSe_2$/NC | 1.0 | 250 | 301 | 1.0 | composite | [1] |
| $FeSe_2$@NC | 0.5 | 100 | 280 | 1.0-1.5 | composite | [2] |
| $FeSe_2$ | 0.4 | 80 | 441 | 1.0-1.2 | composite | [3] |
| ZnSe-$FeSe_2$/RGO | 0.05 | 100 | 363 | / | composite | [4] |
| $FeSe_2$/N-C | 0.2 | 100 | 256 | 1.0 | composite | [5] |
| $FeSe_2$@C NBs | 0.1 | 700 | 221 | / | composite | [6] |
| f-$FePSe_3$/CNT | 0.5 | 1000 | 223 | 0.8 | composite | [7] |

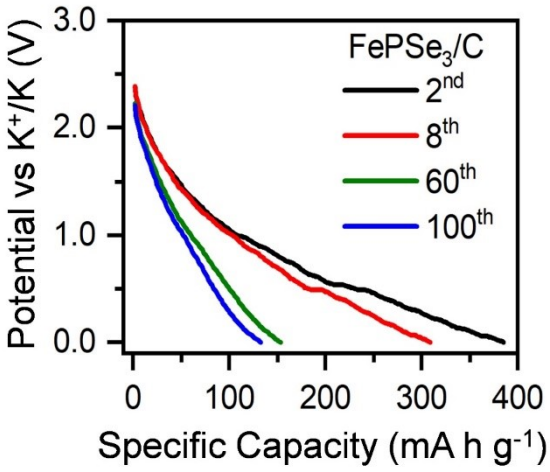


**Figure S19.** The galvanostatic discharge profiles of $FePSe_3$/C at the $2^{nd}$, $8^{th}$, $60^{th}$ and $100^{th}$ cycles at 0.1 A $g^{-1}$ in the voltage range of 0.005-2.8 V.

**Table S5.** The specific capacities of $FePSe_3$-$FeSe_2$/C electrode in three voltage ranges.

| | **2nd cycle** | **8th cycle** | **60th cycle** | **100th cycle** |
|---|---|---|---|---|
| **Voltage range (V)** | **Specific capacity (mA h $g^{-1}$)** | | | |
| **0.005-1.00** | 260.2 | 201.6 | 189.1 | 179.9 |
| **1.00-1.58** | 73.7 | 72.0 | 77.0 | 78.7 |
| **1.58-2.80** | 51.9 | 63.6 | 92.0 | 93.7 |
| **Full range** | 385.8 | 337.2 | 358.1 | 352.3 |

**Table S6.** The capacity increments of $FePSe_3$-$FeSe_2$/C electrode in three voltage ranges.

| | **$\triangle C_{8-2}$** | **$\triangle C_{60-8}$** | **$\triangle C_{100-60}$** |
|---|---|---|---|
| **Voltage range (V)** | **Specific capacity (mA h $g^{-1}$)** | | |
| **0.005-1.00** | -58.6 | -12.5 | -9.2 |
| **1.00-1.58** | -1.7 | 5.0 | 1.7 |
| **1.58-2.80** | 11.8 | 28.4 | 1.7 |
| **Full range** | -48.5 | 20.9 | -5.8 |

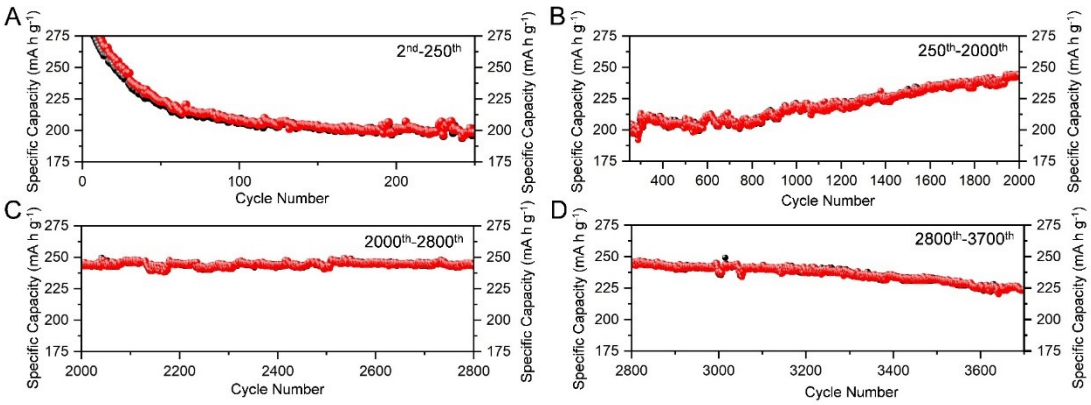


**Figure S20.** Cycling performance of $FePSe_3$-$FeSe_2$/C at a current density of 1.0 A $g^{-1}$ in different cycle intervals: (A) from the 2nd to the 250th cycle, (B) from the 250th to the 2000th cycle, (C) from the 2000th to the 2800th cycle and (D) from the 2800th to the 3700th cycle.

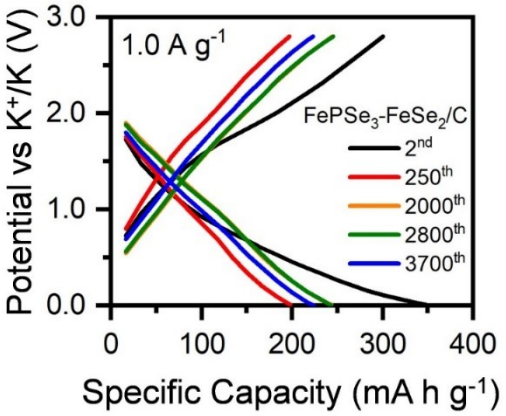


**Figure S21.** The galvanostatic charge/discharge profiles of $FePSe_3$-$FeSe_2$/C at the 2nd, 250th, 2000th, 2800th and 3700th cycles at 1.0 A $g^{-1}$ in 0.005-2.8 V.

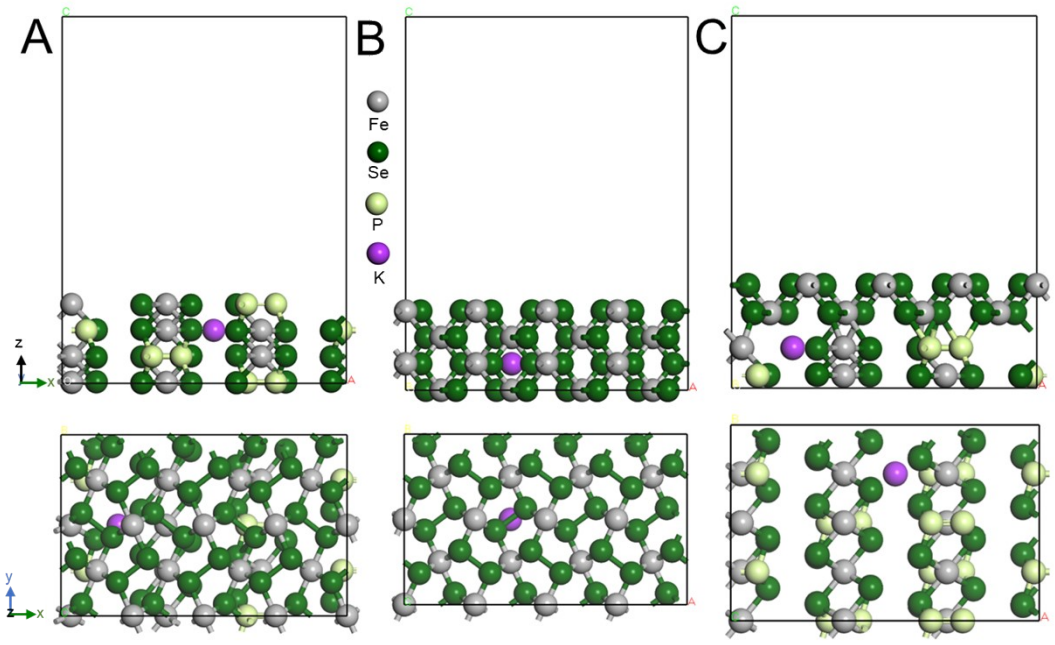


**Figure S22.** Side-view (up) and top-view (down) of built models of (A) $FePSe_3$, (B) $FeSe_2$, and (C) $FePSe_3$-$FeSe_2$.

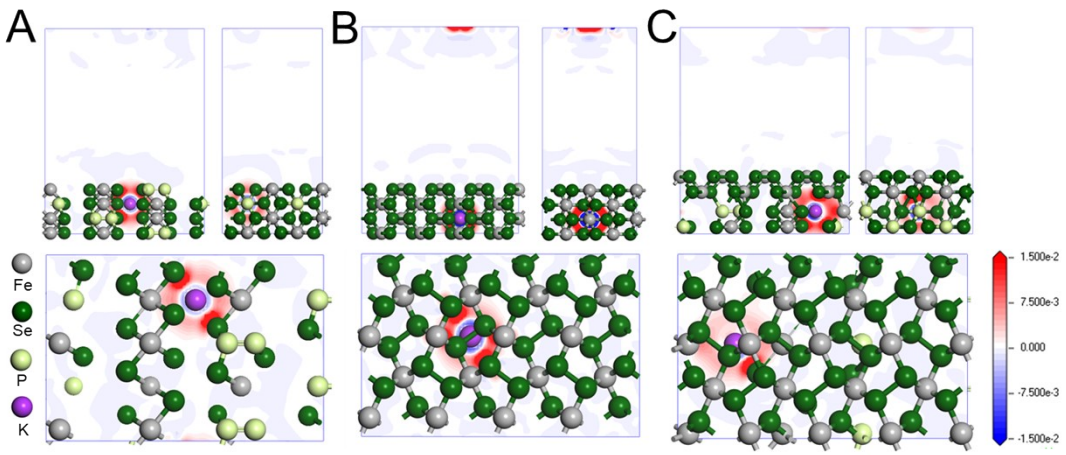


**Figure S23.** Three slices of electron density map of (A) $FePSe_3$, (B) $FeSe_2$, and (C) $FePSe_3$-$FeSe_2$.

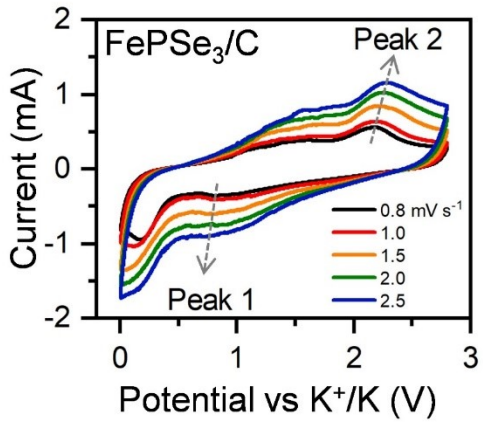


**Figure S24.** CV curves of $FePSe_3/C$ at different scan rates from 0.8 to 2.5 mV $s^{-1}$.

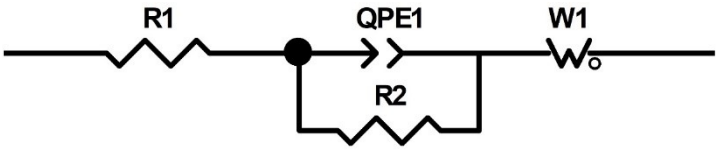


**Figure S25.** Equivalent circuit for measured EIS spectra.

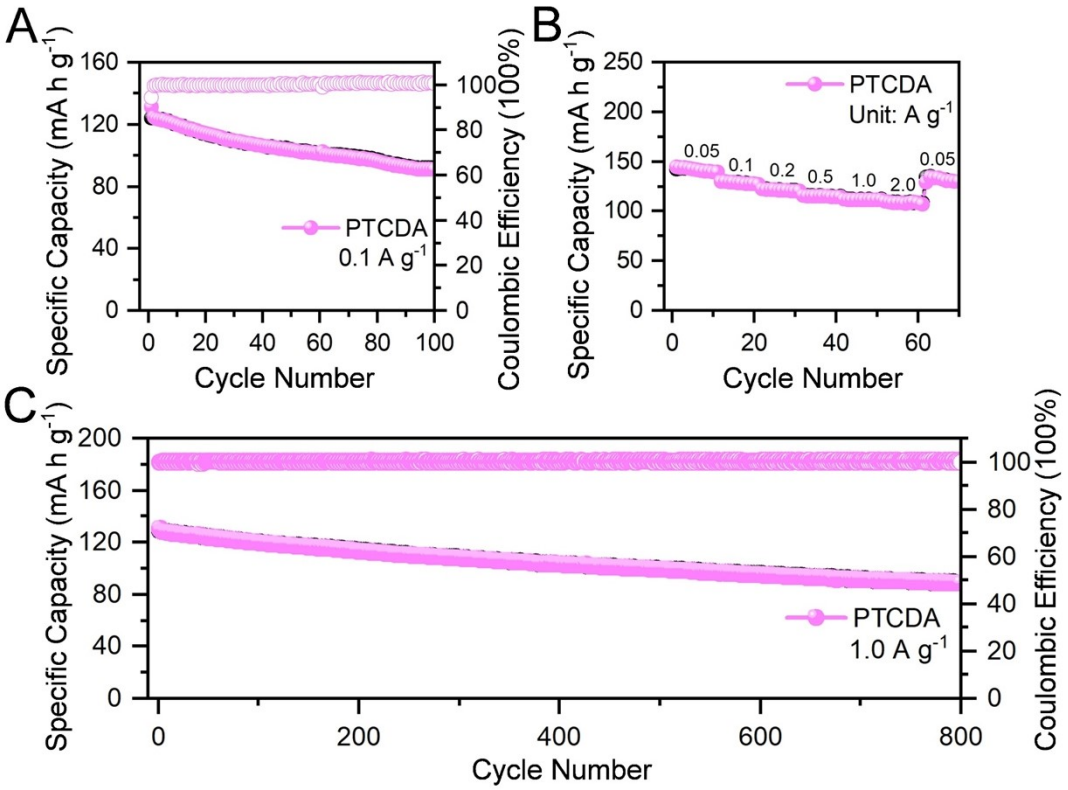


**Figure S26.** (A) Cycling performance, (B) rate performance and (C) long-term cyclic performance of PTCDA half cell in the voltage range of 1.5-3.5 V.

## References


1. Liu, Y. Z.; Yang, C. H.; Li, Y. P.; Zheng, F. H.; Li, Y. J.; Deng, Q.; Zhong, W. T.; Wang, G.; Liu, T. Z., $FeSe_2$/nitrogen-doped carbon as anode material for Potassium-ion batteries. *Chemical Engineering Journal* **2020,** *393*, 124590.

2. Wu, H.; Lu, S.; Xu, S.; Zhao, J.; Wang, Y.; Huang, C.; Abdelkader, A.; Wang, W. A.; Xi, K.; Guo, Y.; Ding, S.; Gao, G.; Kumar, R. V., Blowing Iron Chalcogenides into Two-Dimensional Flaky Hybrids with Superior Cyclability and Rate Capability for Potassium-Ion Batteries. *ACS Nano* **2021,** *15* (2), 2506-2519.

3. Xin, W.; Chen, N.; Wei, Z.; Wang, C.; Chen, G.; Du, F., Self-Assembled $FeSe_2$ Microspheres with High-Rate Capability and Long-Term Stability as Anode Material for Sodium- and Potassium-Ion Batteries. *Chemistry* **2021,** *27* (11), 3745-3752.

4. Yuan, J.; Liu, W.; Zhang, X.; Zhang, Y.; Yang, W.; Lai, W.; Li, X.; Zhang, J.; Li, X., MOF derived ZnSe-$FeSe_2$/RGO Nanocomposites with enhanced sodium/potassium storage. *Journal of Power Sources* **2020,** *455*, 227937.

5. Ge, J. M.; Wang, B.; Wang, J.; Zhang, Q. F.; Lu, B. G., Nature of $FeSe_2$/N-C Anode for High Performance Potassium Ion Hybrid Capacitor. *Advanced Energy Materials* **2020,** *10* (4), 1903277.

6. Liu, C.; Li, Y. J.; Feng, Y. H.; Zhang, S.; Lu, D.; Huang, B. Y.; Peng, T.; Sun, W. W., Engineering of yolk-shelled $FeSe_2$@nitrogen-doped carbon as advanced cathode for potassium-ion batteries. *Chinese Chemical Letters* **2021,** *32* (11), 3601-3606.

7. Huang, Y.-F.; Yang, Y.-C.; Tuan, H.-Y., Construction of strongly coupled few-layer $FePSe_3$-CNT hybrids for high performance potassium-ion storage devices. *Chemical Engineering Journal* **2023,** *451* (4), 139013.